Acta Oceanol. Sin., 2022, Vol. 41, No. 7, P. 1–12
https://doi.org/10.1007/s13131-022-2013-5
http://www.aosocean.com
E-mail: ocean2@hyxb.org.cn

Circulation in the South China Sea is in a state of forced oscillation: Results from a simple reduced gravity model with a closed boundary

Rui Xin Huang[1], Hui Zhou[2, 3, 4*]

[1] Woods Hole Oceanographic Institution, Woods Hole, Massachusetts 02543, USA

[2] Key Laboratory of Ocean Circulation and Waves, Institute of Oceanology, Chinese Academy of Sciences, Qingdao 266071, China

[3] Laboratory for Ocean Dynamics and Climate, Pilot National Laboratory for Marine Science and Technology (Qingdao), Qingdao 266237, China

[4] University of Chinese Academy of Sciences, Beijing 100049, China

Received 10 June 2021; accepted 26 November 2021

Abstract

The South China Sea (SCS) is a narrow semi-enclosed basin, ranging from 4°–6°N to 21°–22°N meridionally. It is forced by a strong annual cycle of monsoon-related wind stress. The Coriolis parameter f increases at least three times from the southern basin to the northern basin. As a result, the basin-cross time for the first baroclinic Rossby wave in the southern part of the basin is about 10-times faster than that in the northern part, which plays the most vitally important role in setting the circulation. At the northernmost edge of SCS, the first baroclinic Rossby wave takes slightly less than 1 year to move across the basin, however, it takes only 1–2 months in the southernmost part. Therefore, circulation properties for a station in the model ocean are not solely determined by the forcing at that time instance only; instead, they depend on the information over the past months. The combination of a strong annual cycle of wind forcing and large difference of basin-cross time for the first baroclinic Rossby wave leads to a strong seasonal cycle of the circulation in the SCS, hence, the circulation is dominated by the forced oscillations, rather than the quasi-steady state discussed in many textbooks.The circulation in the SCS is explored in detail by using a simple reduced gravity model forced by seasonally varying zonal wind stress. In particular, for a given time snap the western boundary current in the SCS cannot play the role of balancing mass transport across each latitude nor balancing mechanical energy and vorticity in the whole basin. In a departure from the steady wind-driven circulation discussed in many existing textbooks, the circulation in the SCS is characterized by the imbalance of mechanical energy and vorticity for the whole basin at any part of the seasonal cycle. In particular, the western boundary current in the SCS cannot balance the mass, mechanical energy, and vorticity in the seasonal cycle of the basin. Consequently, the circulation near the western boundary cannot be interpreted in terms of the wind stress and thermohaline forcing at the same time. Instead, circulation properties near the western boundary should be interpreted in terms of the contributions due to the delayed wind stress and the eastern boundary layer thickness. In fact, there is a clear annual cycle of net imbalance of mechanical energy and vorticity source/sink. Results from such a simple model may have important implications for our understanding of the complicated phenomena in the SCS, either from *in-situ* observations or numerical simulations.

Key words: South China Sea, ocean circulation, annual cycle, first baroclinic Rossby wave propagation, western boundary current, forced ossilation

Citation: Huang Rui Xin, Zhou Hui. 2022. Circulation in the South China Sea is in a state of forced oscillation: Results from a simple reduced gravity model with a closed boundary. Acta Oceanologica Sinica, 41(7): 1–12, doi: 10.1007/s13131-022-2013-5

1 Introduction

The circulation in South China Sea (SCS) shares many important characters with the circulation in the world oceans. Circulation in the SCS can be separated into two components, the wind-driven circulation and the thermohaline circulation. Our study in this note is focused on the wind-driven circulation, which has been studied in many previous publications (Wyrtki, 1961; Shaw et al., 1999; Chu et al., 1999; Qu, 2000; Fang et al., 2002; Yang et al., 2002; Gan et al., 2006; Wang et al., 2006).

One of the most important characters of the wind-driven circulation in the SCS is that the strong annual cycle related to the South Asia monsoon. In fact, wind stress in the SCS can completely reverse its direction during a typical annual cycle. The time evolution during the annual cycle is an important aspect of

Foundation item: The Strategic Priority Research Program of the Chinese Academy of Sciences under contract No. XDB42000000; the National Natural Science Foundation of China under contract No. 41876009.
*Corresponding author, E-mail: zhouhui@qdio.ac.cn

the circulation.

There have been many papers published about the time-dependent circulation in the ocean, e.g., Pedlosky (1965). Among the many aspects of circulation in the SCS, the structure and variability of the western boundary current (WBC) is a hot topic. For example, recently, He et al. (2020) gave a detailed review about the progress made in the study of WBC in the SCS. In addition, there is a recent publication by Liang (2017), in which the author argued that the time-varying nature of monsoon may suppress the WBC. Note that both the papers by Pedlosky (1965) and Liang (2017) are focused on the Quasi-Geostrophic (QG) theory of the wind-driven circulation. While QG theory is a very powerful tool in studying oceanic circulation, there are some intrinsic limitations of the theory. In particular, the long first baroclinic mode Rossby wave speed in the QG theory is proportional to β/f_0^2 (where f_0 is the Coriolis parameter at a fixed latitude and β the fixed meridional gradient of the Coriolis parameter); thus, it is constant within the whole model basin. As will be shown shortly, in a simple reduced gravity model on a β-plane, the long Rossby wave speed is proportional to β/f^2 (where f is the Coriolis parameter varing with latitude and β the meridional gradient of f). For the case of SCS, f increases at least three times from the southern basin to the northern basin. As a result, the Rossby wave speed in the northern part of the basin is about 10 times slower than that in the southern part of the basin. As will be discussed in this study, the dramatic difference in the basin-cross time of Rossby waves is one of the most important factors regulating the seasonal cycle of circulation in the SCS.

The rest of this note is organized as follows. Section 2 is focused on the basic equations for a reduced gravity model, including the balance of energy and vorticity. Section 3 is the model discription, including the model boundary setting and wind stress forcing used in different numerical experiments, and the corresponding results. Section 4 is the conclusions.

2 Basic equations

An idealized 1.5-layer reduced gravity model on a β-plane is formulated for the SCS, in this model the lower layer is assumed infinitely deep and thus motionless. The basic equations for the upper layer are

$$hu_t + h(uu_x + vu_y) - fhv = -g'hh_x + \tau^x/\rho_0 + A\nabla_h{}^2(hu) - \kappa u, \quad (1)$$

$$hv_t + h(uv_x + vv_y) + fhu = -g'hh_y + \tau^y/\rho_0 + A\nabla_h{}^2(hv) - \kappa v, \quad (2)$$

$$h_t + (hu)_x + (hv)_y = 0, \quad (3)$$

where h is the layer depth, $\vec{u} = (u, v)$ is the horizontal velocity, ρ_0 is the reference density, A is the lateral friction parameter, and κ is the bottom friction parameter.

2.1 *Energy balance*

Energy balance can be derived by $u\times$Eq. (1) $+v\times$Eq. (2),

$$hK_t + h\vec{u}\cdot\nabla_h(K+P) = W, \quad (4)$$

where

$$K = \frac{u^2+v^2}{2},\ P = g'h \quad (5)$$

are the kinetic energy and potential energy, respectively.

$$W = \frac{1}{\rho_0}(u\tau^x + v\tau^y) - \kappa(u^2+v^2) + A[u\nabla_h{}^2(hu) + v\nabla_h{}^2(hv)] \quad (6)$$

is the work of wind stress and dissipation by bottom/lateral friction. Based on the continuity equation (Eq. (3)), the total volume integrated over the model domain of a closed basin is constant with time. However, the total kinetic energy can change with time.

Using Eq. (3), Eq. (4) is further transformed to the following form,

$$(hK)_t + \left(\frac{g'h^2}{2}\right)_t + \nabla_h[h\vec{u}(K+P)] = W. \quad (7)$$

Assuming the lateral boundary is a solid wall, integrating Eq. (7) over the whole model domain, the contribution from the third term on the left-hand side vanishes. Thus, we have the following equation for the whole model domain,

$$\iint_A \left[(hK)_t + \left(\frac{g'h^2}{2}\right)_t\right]\mathrm{d}A = \iint_A W\mathrm{d}A. \quad (8)$$

Therefore, the total kinetic energy and potential energy in the model ocean can change due to the net work (source minus sink) imposed on the model ocean.

In fact, due to the seasonal cycle of wind stress, the total work from wind and dissipation due to friction may change with the season, thus leading to the seasonal change of net kinetic energy and potential energy of the model ocean.

2.2 *Vorticity balance*

Dividing Eqs (1) and (2) by h, then cross-differentiating and subtracting lead to

$$(v_x - u_y)_t + \nabla_h(q\vec{u}) = C, \quad (9)$$

where $\zeta = v_x - u_y$, $q = f + \zeta$ are the relative vorticity and total vorticity, respectively.

$$C = \left(\frac{\tau^y}{\rho_0 h} - \frac{\kappa v}{h} + \frac{A}{h}\nabla_h{}^2(hv)\right)_x - \left(\frac{\tau^x}{\rho_0 h} - \frac{\kappa u}{h} + \frac{A}{h}\nabla_h{}^2(hu)\right)_y \quad (10)$$

is the source/sink of vorticity.

Assuming the lateral boundary is a solid wall, integrating Eq. (9) over the whole model domain, and the contribution from the divergence term vanishes. Thus, we have the following equation for the whole model domain:

$$\iint_A (v_x - u_y)_t\mathrm{d}A = \iint_A C\mathrm{d}A. \quad (11)$$

3 Results from the model

In this study, we will use a simple rectangular model (6°–22°N, 110°–120°E) to represent the South China Sea, with closed boundary. The model is forced by the monthly climatology wind data derived from GODAS monthly wind stress data between 1980 and 2019 (Climate Prediction Center-NCEP Global Ocean Data Assimilation System (noaa.gov)). The GODAS data is on a 1°×(1/3)° resolution, and is linearly interpolated on a (1/3)°×

(1/3)° grid for our model. We identified the climatological mean seasonal cycle of the wind stress over the model domain, then we constructed three types of wind stress based on this climatology as shown in Table 1.

First, we generate a zonally mean monthly zonal wind stress data, $\overline{\tau^x(y,m)}^x$, which is the wind forcing for our first experiment, and the seasonal cycle of this wind stress data is shown in Fig. 1a. Similarly, the meridionally mean meridional wind stress data, $\overline{\tau^y(x,m)}^y$ is generated, and shown in Fig. 1b. The above two types of wind stress data ($\overline{\tau^x(y,m)}^x$, $\overline{\tau^y(x,m)}^y$), compose the wind forcing for our second experiment. Third, the two-dimensional wind stress data, ($\tau^x(x,y,m)$, $\tau^y(x,y,m)$), generated from the original wind stress data by multi-year mean (figure not included), is used in our third experiment.

Using these indealized wind stresses as forcing, we run the following numerical experiments (Exps 1–7) for the model ocean as listed in Table 2, which also includs the geometric settings, such as the zonal and meridional ranges of the model ocean, the wind stress data used in each experiment and the duration of the experiments. Exps 1–3 are designed to test the sensitivity of the seasonal cycle of circulation in the SCS to different wind forcings. Exps 4 and 5 are used to demonstrate the role of Rossby wave speed in adjusting the seasonal cycle of the circulation for different latitudinal ranges in the SCS. Exps 6 and 7 are used to discuss the influence of zonal width of the basin in regulating the seasonal cycle of the SCS circulation.

The model is a reduced gravity model on a β-plane. Since the model is run on a relatively low resolution of (1/3)°×(1/3)°, it is based on the B-grid and the traditional leap-frog scheme in time march. The details of the numerical model is referred to Huang (1986). The reduced gravity is g'=0.025 m/s², A=1 000 m²/s, and k=1.5×10^{-4} m/s. Each numerical experiment is spin up from an initial state of a rest ocean with the mean layer thickness of 200 m and run at least for 20 years before diagnosis for the model output. As will be shown shortly, the long Rossby waves take about 10 months to move across such a narrow basin at 20°N. Due to the large meridional model domain setting, Exps 5, 6 and 7 were run for longer time, as shown in Table 2; thus, these experiments should reach a quasi-steady state of the periodic motions.

Table 1. Idealized wind stress data used in the model experiments

	Zonally mean zonal wind stress	Zonally mean zonal wind stress and meridionally mean meridional wind stress	Two-dimensional wind stress
Expression	$\overline{\tau^x(y,m)}^x$	$\overline{\tau^x(y,m)}^x$, $\overline{\tau^y(x,m)}^y$	$\tau^x(x,y,m)$, $\tau^y(x,y,m)$

Note: m=(1, ..., 12) is the month.

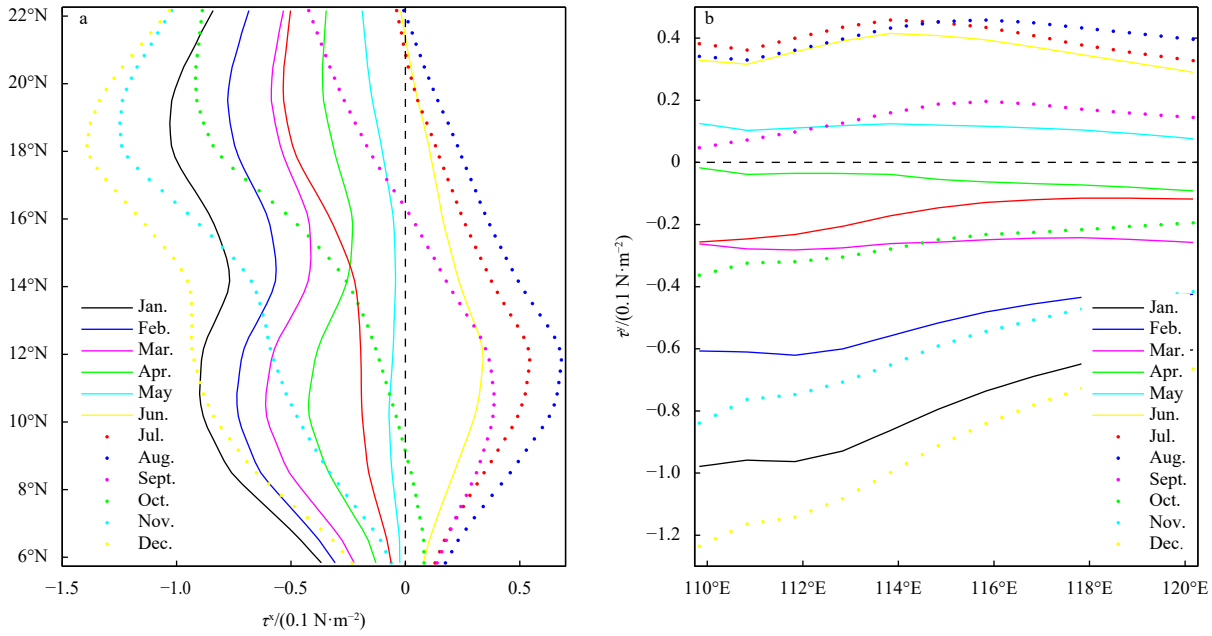

Fig. 1. Idealized monthly mean wind stress for the model. a. Zonal wind (independent of longitude); b. meridional wind (independent of latitude); based on Global Ocean Data Assimilation System data.

Table 2. Experiment design

Experiments	Meridional range	Zonal range	Wind stress	Run duration/a
Exp. 1	6°–22°N	110°–120°E	$\overline{\tau^x(y,m)}^x$	20
Exp. 2	6°–22°N	110°–120°E	$\overline{\tau^x(y,m)}^x$, $\overline{\tau^y(x,m)}^y$	20
Exp. 3	6°–22°N	110°–120°E	$\tau^x(x,y,m)$, $\tau^y(x,y,m)$	20
Exp. 4	0°–16°N	110°–120°E	$\overline{\tau^x(y,m)}^x$	20
Exp. 5	16°–32°N	110°–120°E	$\overline{\tau^x(y,m)}^x$	40
Exp. 6	6°–22°N	110°–170°E	$\overline{\tau^x(y,m)}^x$	60
Exp. 7	6°–22°N	480°	$\overline{\tau^x(y,m)}^x$	400

Note: Here we expand the width of the model ocean basin to an unrealistic 480°.

The monthly mean $\overline{\tau^x(y,m)}^x$ can generate an idealized circulation in the SCS, which is a typical characteristic of the SCS (Fig. 2a). The Ekman pumping induced by such an idealized wind stress shows an obvious seasonal cycle (Fig. 2b). In spring, Ekman pumping is positive at the southern edge of the basin, but it is negative at the middle of the basin. The situation is reversed during the summer season, with negative Ekman pumping at the southern edge, but positive for the mid and high latitude parts of the model basin; then the pattern reverses again for the winter season. Overall, the Ekman pumping is negative for January, February and March, April is the month of switching, and the overall pumping rate is positive for the rest of the year, as shown in Fig. 2c. The annual mean WSC shows two positive bands around 14°–19°N and the southern basin south of 9°N, two negative bands north of 19°N and around 9°–14°N (Fig. 2b).

3.1 *Circulation diagnosis of the model*

The model ocean is in a state of forced oscillation, and this can be clearly seen from both the layer thickness and boundary current transport. The layer thickness distribution in winter (January) and summer (July) from Exps 1, 2 and 3 is shown in Fig. 3. In Jannuary, there is a strong anticyclonic gyre in the northwest part of the model basin for these numerical experiments. In the northeast part of the basin there is a cyclonic gyre, which is confined to the eastern basin in Exp. 1 (Fig. 3a), but it expands into the basin interior in Exp. 2 (Fig. 3b), and in particular, this cyclonic gyre is well-developed in Exp. 3 (Fig. 3c). The anticyclonic gyre in the winter season of this model ocean is closely linked to the negative wind stress curl in the northern part of the basin. In reality, the winter circulation in the northern part of SCS is dominated by a cyclonic gyre. As will be explained in Part II of this study, the anticyclonic gyre in winter in this model ocean is an artifact due to the cut off of the South China Sea throughflow (SCSTF) and treating the shallow coast regime in the northwest part of SCS and a deep ocean regime. In summer (July) the model circulation is dominated by a cyclonic gyre in the north and an anticyclonic gyre in the eastern and southern parts of the model basin (Figs 3d–h).

The seasonal cycle of circulation is shown by the volumetric transport along the eastern/western boundary, defined by three grids adjacent to the boundaries, which represents the eastern/western boundary current (EBC/WBC) in the model. Figure 4 show the transports of the two boundary currents derived from the three experiments. Although the patterns are slightly different, the overall structures remain the same in all these three cases.

The design of three types of wind forcing in these experiments aims to emphasize the dominant role of the large difference between the speed of the forced long first baroclinic Rossby waves in the southern and northern basins. As shown in the Appendix, the speed of the free long Rossby waves in such a reduced gravity model is

$$C(y) = \beta g' H / f^2. \tag{12}$$

In the present case, the layer thickness H is nearly constant; thus, the wave speed is inversely proportional to the squared Coriolis parameter f. For the standard case, f is increased 3 times from the southern edge to the northern edge of the model ocean; hence, near the southern boundary the wave speed is about 10 times faster than that near the northern boundary.

Based on observations, the westward propagation speed of forced Rossby waves is estimated at 5 cm/s for the latitude band of 18°–22°N in South China Sea (Yang and Liu, 2003), and numerical calculation based on stratification also support this estimation (Cai et al., 2008). Consequently, the basin-cross time is about 1 month near the southern boundary, but it is about 11 months

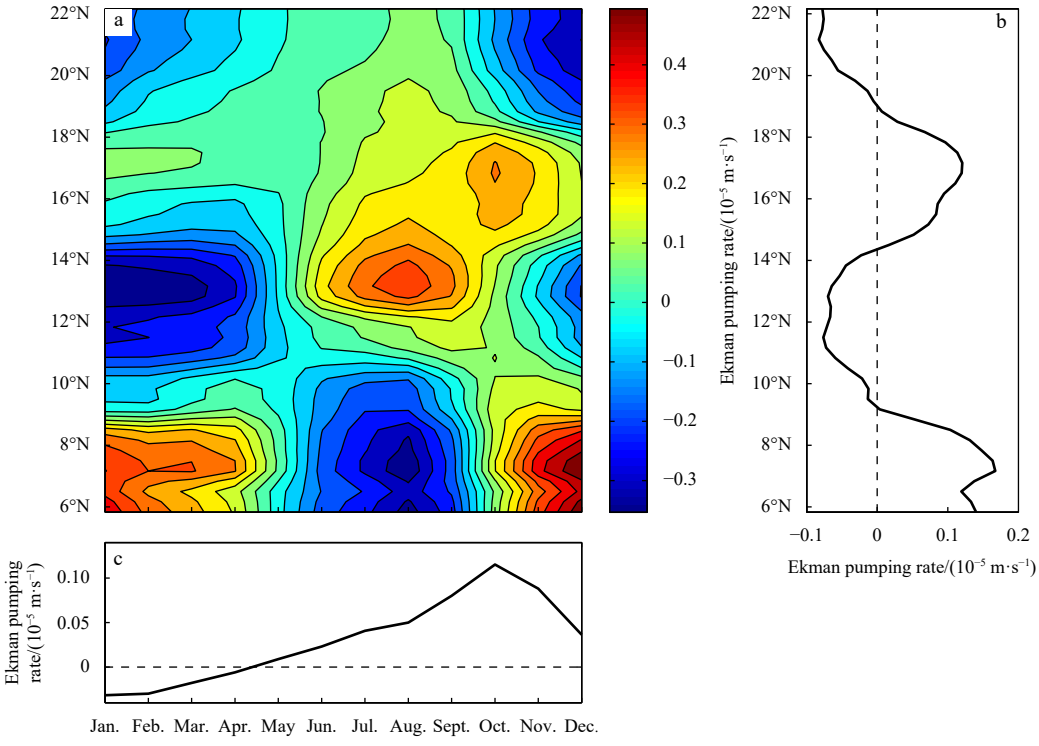

Fig. 2. The time-latitude diagram of the climatological monthly mean Ekman pumping rate for the model forced by the zonally mean zonal wind stress only (a); the annual mean Ekman pumping rate (b); the basin mean Ekman pumping rate (c).

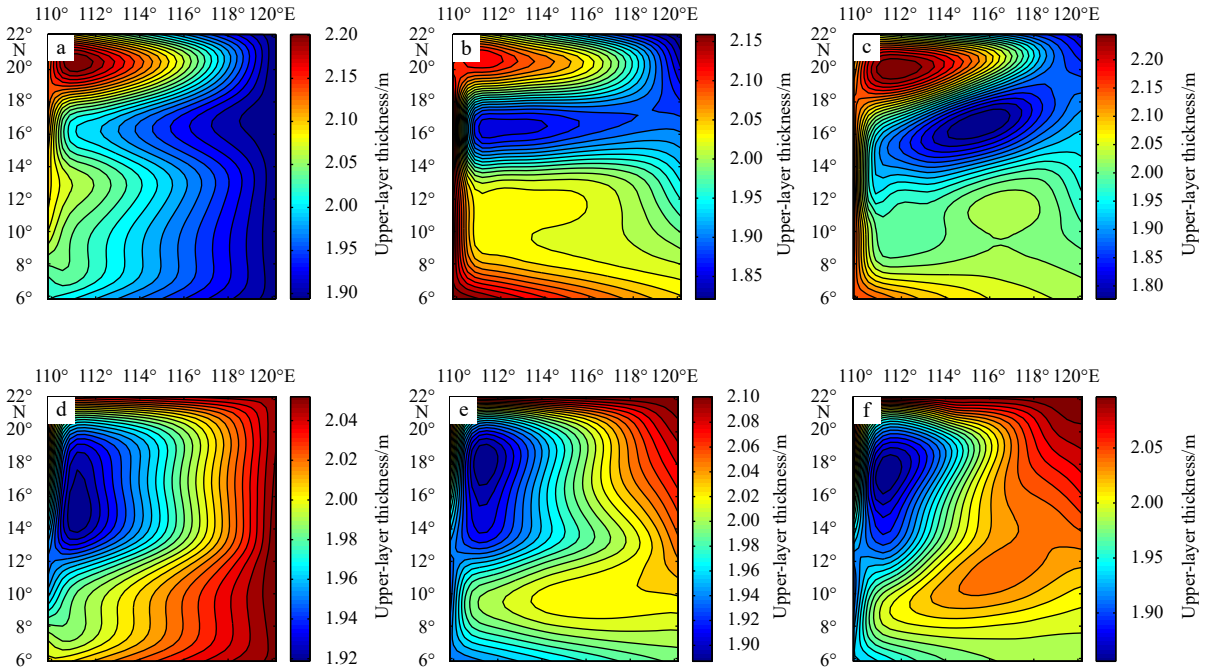

Fig. 3. Layer depth in January (a–c) and July (d–f) for the simple model forced by zonally mean zonal wind (a, d, Exp. 1), by zonally mean zonal wind and meridionally mean meridional wind (b, e , Exp. 2) and 2D wind (c, f , Exp. 3).

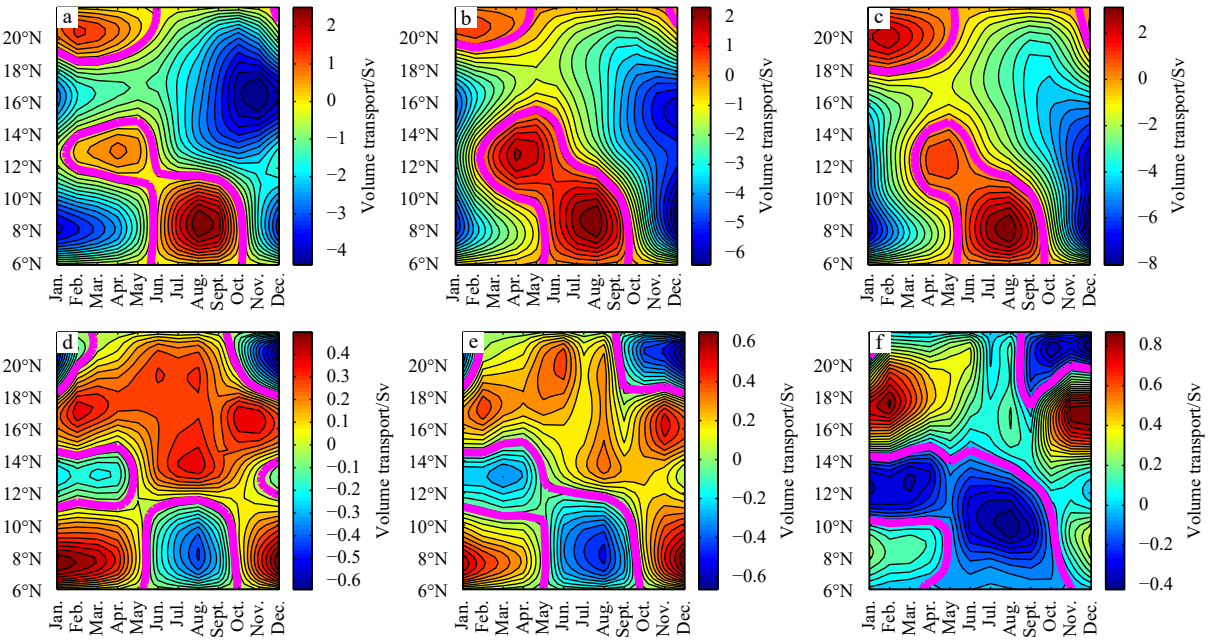

Fig. 4. Western boundary current transport (a–c) and eastern boundary current (d–f) for a simple model forced by zonally mean zonal wind (a, d, Exp. 1), by zonally mean zonal wind and meridionally mean meridional wind (b, e, Exp. 2) and 2D wind (c, f, Exp. 3). The magenta curves indicate the zero contours (1 Sv=10^6 m^3/s).

near the northern boundary (middle panels of Fig. 5).

The speed of long Rossby waves in the model can be diagnosed from the model output. For example, using the time evolution of the layer thickness along a given latitude, we can estimate the signal speed, as shown in Fig. 6. For example, along 19.66°N, there are clear signs that the layer thickness propagates westward with a speed of approximately 4.79 cm/s; at a lower latitude section along 12.33°N, the corresponding signal speed can reach about 12.17 cm/s.

The speed of long Rossby waves is a critically important parameter in regulating the seasonal cycle in the SCS. Because the Sverdrup relation discussed in many textbooks or publications are valid for the steady circulation only. For the time-dependent circulation, the finite speed of signal propagation in the form of long Rossby waves must be included. In a linearized model, the corresponding delayed Sverdrup relation is given by

$$h = h\left(x_e, y, t + \frac{x - x_e}{C(y)}\right) - \frac{f^2}{\beta g' H}\int_x^{x_e} w_e\left(x', y, t + \frac{x - x'}{C(y)}\right)\mathrm{d}x', \tag{13}$$

where $\Delta t = (x - x_e)/C(y)$is the time for the Rossby waves to move from the eastern boundary x_e to a given station x, and this time is inversely proportional to the wave speed, which is a function of latitude y, see Appendix for details. According to Eq. (13), at a time t, the layer thickness at station x is the sum of two terms. First, the eastern boundary layer thickness at the previous time Δt. The second term is a delayed Ekman pumping rate integrated over the time of Δt, hence it includes wind stress contribution for the entire time period of [t–Δt ,t]. For example, for a station close to the southern edge and near the western boundary, the layer thickness depends on the information over the past month. However, for a station close to the northern boundary and near the western boundary, the layer thickness depends on the information over the past 10 months.

Therefore, circulation properties for a station in the model ocean are not solely determined by the forcing at that time instance only; instead, they depend on the information over the past months, as demonstrated by Eq. (13). Both the corresponding eastern boundary layer thickness at the previous time and the delayed Sverdrup term integrated over the past months contribute to the regulation of circulation properties in the basin interior.

Note that wave speed calculated from Eq. (12) is based on the

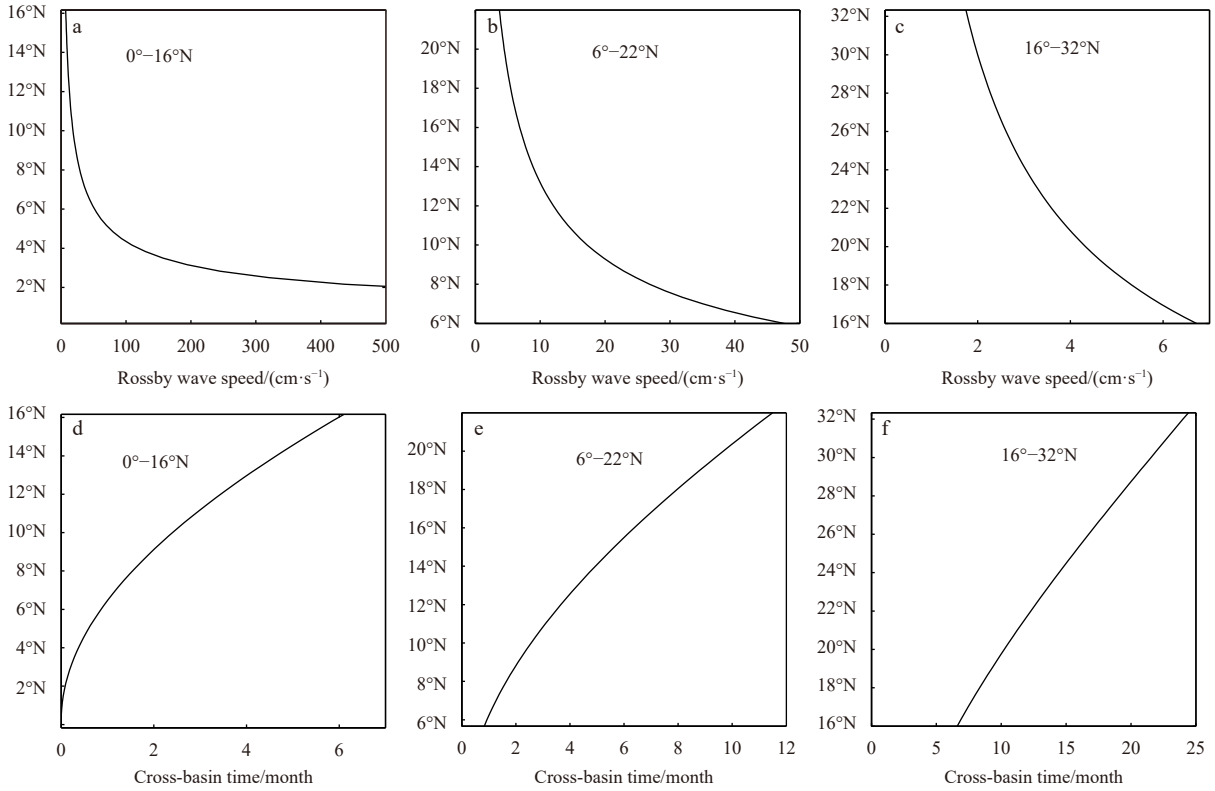

Fig. 5. Rossby wave speed (a–c) and the cross-basin time (d–f) for the model located between 0°–16°N (Exp. 4, a, d); the model located between 6°–22°N for Exp. 1 (b, e) and the model located between 16°–32°N for Exp. 5 (c, f).

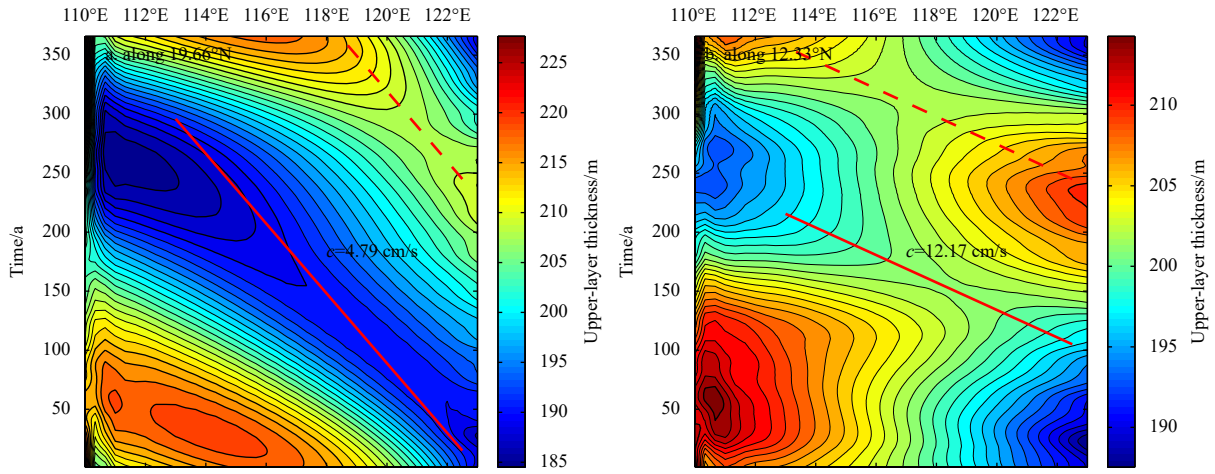

Fig. 6. Time evolution of layer depth for the model forced by zonal wind stress only (Exp. 1). The dashed and solid red lines indicate the corresponding signal speed.

simple theoretical formula for the free Rossby waves; in this formular othe facts are omitted, such as the friction and external wind forcing. In fact, waves appears in the model ocean or real world should be classified as forced Rossby waves, and their speed is regulated by external forcing as well. For example, the SCSTF enters the SCS through the Luzon Strait around the latitude of 20°N but leaves near the equator. Thus, the SCSTF brings in positive vorticity to the SCS (Yang and Price, 2000). The baroclinicity and the budget of vorticity inside the basin may be alterd by the formation of a cyclonic circulation in the basin to balance the net positive vorticity brought in by the SCSTF, which needs further study in the future.

3.2 *Diagnosis of the role of Rossby wave speed in model ocean*

To demonstrate the critically important role of Rossby wave speed we carried out one set of idealized model experiments. In addition to the original geographic setting, we added two more model basins, which have the same geometry, but the northern and southern boundaries of the model are moved meridionally. As shown in in the left column of Fig. 7, in the first case, the model ocean is moved to a new geographic location of 0°–16°N. Due to the change in latitude, the Rossby wave speed increases and the corresponding basin-cross time is reduced to 0–6 months. When the model basin is moved to 16°–32°N, the Rossby wave speed is noticeably reduced and the basin-cross time is greatly increased to 6–24 months (Figs 7c, f).

Although these model oceans are forced by the same zonal wind, the seasonal cycle in the model ocean is different. A simple way to demonstrate the changes in the seasonal cycle is to plot the monthly mean volumetric transport. As shown in Fig. 7, the modelled volumetric transports of the western and eastern boundary currents fluctuate differently depending on the latitudal bands of the basin. For example, the shift month from southward to northward (northward to southward) transport of the WBC/EBC in the southern basin delays with the increasing latitudinal range of the basin. Meanwhile, the maximum transport reaches 2.98 Sv for the 0°–16°N basin location, while it decreases to 1.69 Sv for the 16°–32°N basin location (Table 3).

3.3 *Volumetric transport*

Although the total volume of warm water in the model ocean is constant in time, the amount of water in any specific part of the model basin is not constant. Take Exp. 2 as an example, at each latitudinal band, the zonally integrated layer thickness is not constant. As shown in the left panel of Fig. 8, in January there is more than averaged amount of water in the southern basin, but there is water deficit in the northern part of the basin. This situation is gradually changed, and in summer, there is water deficit in the southern basin and excessive amount of water in the northern basin.

The warm water is actually transported within the model basin, and this can be calculated by integrating the volumetric transport across each latitude. As shown in Fig. 8b, for the most part of the model basin, there is a northward volumetric transport for the first half of the year, with a maximum value of 0.6 Sv. Starting from August, there is a southward volumetric transport in the basin, which reach the minimum value of –0.8 Sv.

Similarly, along each longitudinal band the meridional integrated layer thickness is not constant, the corresponding deviation from the annual mean is shown in Fig. 9a. In January, there

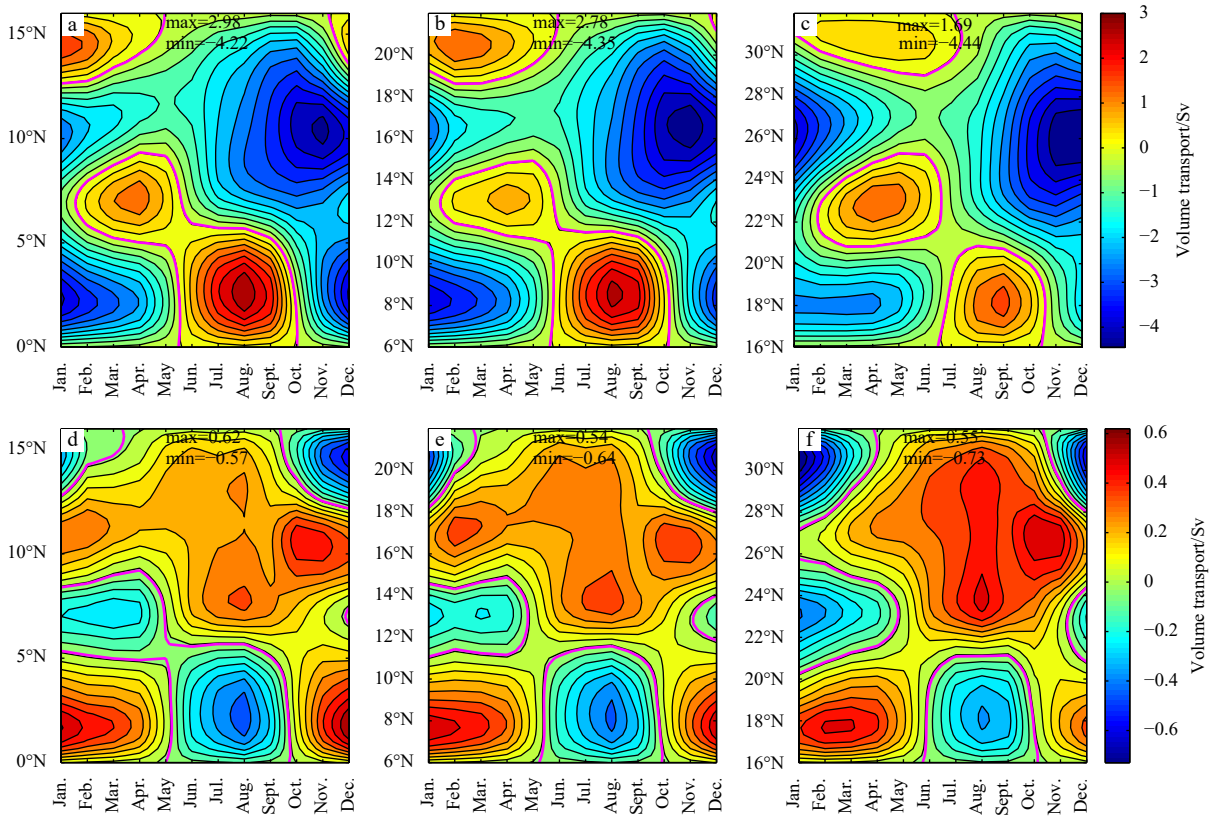

Fig. 7. Volumetric transport of the western boundary current (a–c) and eastern boundary current (d–f). Left column for the model located between 0°–16°N (Exp. 4); middle column for the model located between 6°–22°N (Exp. 1); right column for the model located between 16°–32°N (Exp. 5). The magenta curves indicate the zero contours (1 Sv=10^6 m^3/s).

is excess amount of water in the western basin, and deficit of water in the eastern basin. As time progress, the anomaly gradually declines and the sign flips around summer time. The corresponding zonal volumetric transport can be diagnosed by integration along each longitudinal band. As shown in Fig. 9b, there is a large amount of volumetric transport in the zonal direction, and it reaches the maximum value of 0.8 Sv in June. The zonal transport flips sign and it reaches the minimum value of –0.6 Sv in October.

There is an important implication of the volumetric transport diagnosed from this idealized reduced gravity model. Although one of the basic assumptions in the reduced gravity model is that the lower layer is very deep and motion is very slow and thus the pressure gradient in the lower layer is zero. However, a careful reasoning suggests that the total transport may not be zero because a very small velocity multiplied by a very thick layer may lead to a finite amount of transport in the lower layer. In fact, the sea level in the ocean is kept nearly constant, and it varies within the order of 1 m. Since there is a large amount of water transport in the upper layer, there should be a volumetric flux in the lower layer, which nearly compensating the flux in the upper layer. Therefore, for the cases discussed in Figs 8 and 9, the volumetric transports in the upper layer imply that there should be reverse compensated fluxes below the interface.

3.4 *Balance of mechanical energy and vorticity*

In the classical theory of wind-driven circulation, the western boundary current plays an important role in balancing mass, mechanical energy and vorticity, e.g., Stommel (1948) and Huang (2010). We have discussed the mass balance in the discussion above, and in this subsection, we will discuss the balance of mechanical energy and vorticity.

The fundamental laws governing the wind-driven circulation are balance of mass, mechanical energy and vorticity. The essential part of the mechanical energy balance is the wind stress work input to the model ocean and the dissipation through bottom friction and lateral friction, as shown in Eq. (6). The annual cycle of mechanical energy balance is shown in Fig. 10 for Exp. 1 (forced by zonal wind stress only) and Exp. 3 (forced by two-dimensional wind stress). The black curves show the mechanical energy input to the model ocean. Note that wind stress energy input can be negative for part of the basin where the current is flowing against the local wind. This term reaches its annual minimum in May, and it is maximum in December. The dissipation due to bottom friction and lateral friction is depicted by the blue and green curves. There is clearly an imbalance for each month, as depicted by the red curves. As emphasized repeatedly, the circulation under the seasonal cycle of wind cannot reach a steady state. As a result, the circulation is in a state of forced oscillation; thus, mechanical energy for the whole basin cannot completely balanced for each month. For the case associated with Exp. 3, the balance of mechanical energy is quite similar to the case of Exp. 1, but each term is about 3 times larger (scales are different in Figs 10a, b).

Similarly, the vorticity balance of the model can be diagnosed from the model output. As shown in Fig. 11 for Exp. 1, each month wind stress imposes both positive and negative vorticity into the model ocean, depicted by the black and blue curve in Fig. 11, and the total vorticity input is depicted by the red curve. Overall, the vorticity input into the model ocean is positive, and it is minimum in summer, but it is maximum in October and November. On the other hand, both the bottom friction and lateral friction work as negative source of vorticity, i.e., they take out the positive vorticity imposed by wind stress, and balance the vorticity in the model ocean. Once again, for an individual

Table 3. Volumetric transport of the western/eastern boundary current (WBC/EBC) for three geographic settings of the model ocean

	Western boundary transport			Eastern boundary transport		
Experiment	Exp. 1	Exp. 4	Exp. 5	Exp. 1	Exp. 4	Exp. 5
Basin location	6°–22°N	0°–16°N	16°–32°N	6°–22°N	0°–16°N	16°–32°N
Maximum/Sv	2.78	2.98	1.69	0.54	0.62	0.55
Minimum/Sv	–4.35	–4.22	–4.44	–0.64	–0.57	–0.73

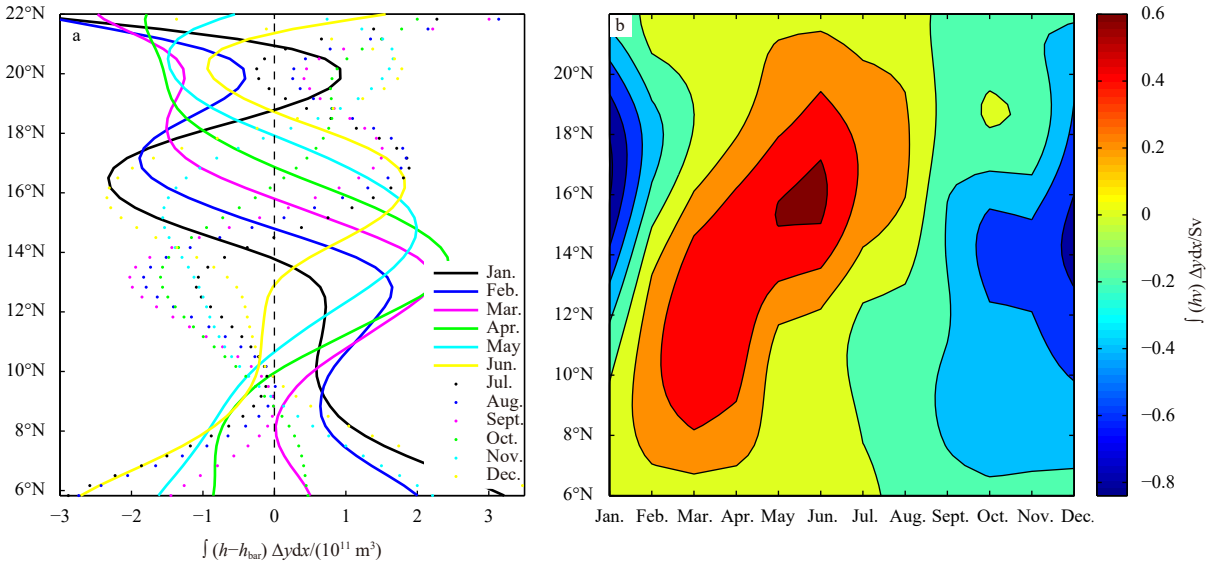

Fig. 8. Experiments forced by idealized monthly zonal/meridional wind (Exp. 2). a. Total volumetric anomaly at each latitude band; b. zonally integrated monthly mean meridional volumetric flux (1 Sv=10^6 m^3/s); bar is the mean thickness of the upper layer.

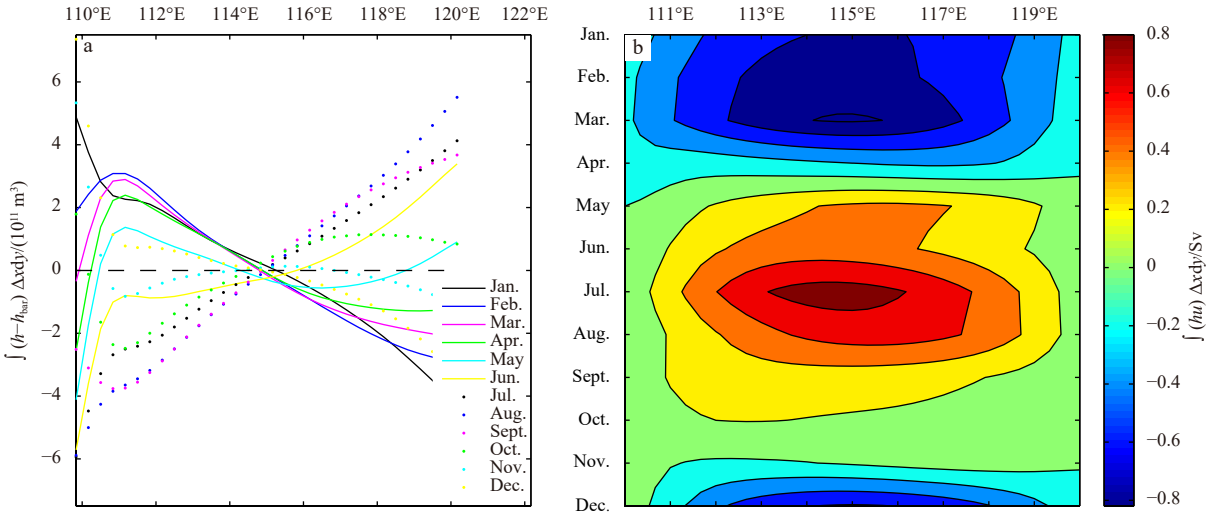

Fig. 9. Experiments forced by idealized monthly zonal/meridional wind (Exp. 2). a. Total volumetric anomaly at each longitude band; b. meridionally integrated monthly mean zonal volumetric flux (1 Sv=10^6 m^3/s).

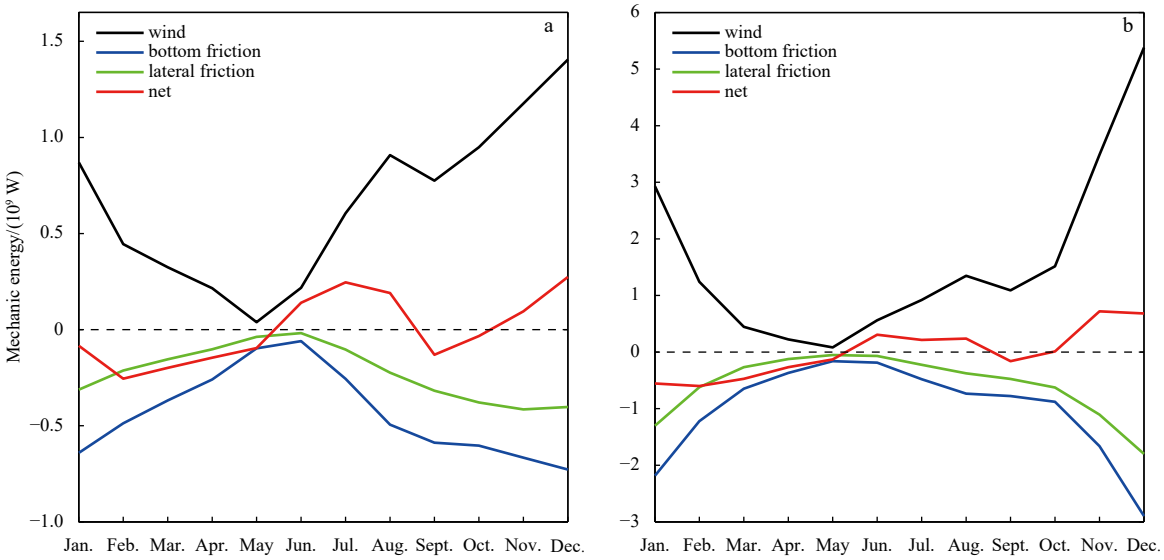

Fig. 10. Annual cycle of mechanic energy balance. a. For the model forced by zonal wind stress only (Exp. 1); b. for the model forced by two-dimensional zonal/meridional wind (Exp. 3).

month, total vorticity is imbalanced, as shown by the non-zero net vorticity (red dashed curve). It is to note that the simple sum of imbalance for these twelve months is not zero. Such a small annual imbalance of vorticity may be due to the numerical errors accumulated in the numerical model and the simple 12-day sampling of the model.

3.5 *Experiments of a zonally extended model ocean*

In addition, we carried out a series of numerical experiments, in which the northern and southern boundaries are fixed at 6°N and 22°N, but the width of the model ocean is extended into 60° (Exp. 6) and 480° (Exp. 7). The same simple zonal wind stress is applied to all these model oceans. The corresponding wave speed and basin-cross time are shown in Fig. 12. The case for the basin with 480° width is a far cry idealization, and it is beyond the reality on the Earth. In such an extreme case, it takes 44 years for the signals to move across the basin (Fig. 12b).

People may speculate that for such a long basin-cross time,

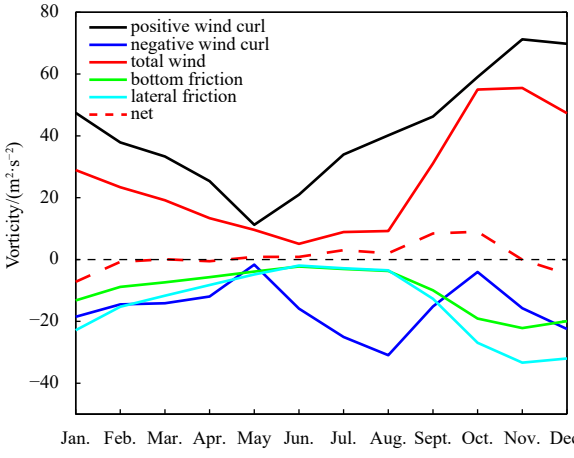

Fig. 11. Vorticity balance for the model forced by zonal wind stress only (Exp. 1).

the delayed Sverdrup relation will give a virtually quasi-steady signal for the basin interior resulting from the 44-year averaging. However, the model results show that there is still a clearly defined annual cycle of the circulation as indicated by the volumetric transport along the western and eastern boundaries shown in Figs 13 and 14. Note that the case with a 480° wide basin, the solution reaches an extreme situation that the upper layer outcrops in the southern part of the eastern boundary, and this is depicted as the blank regime shown in Fig. 14f. Note that the numerical model used in this study is based on a positive-definite scheme, so that the outcrop line can be handled accurately (Huang, 1986). Nevertheless, the seasonal cycle of the model is outstanding for all these cases.

4 Conclusions

Wind-driven circulation in the SCS is characterized by strong annual cycle of wind stress associated with the southeast monsoon. Another important character of SCS circulation is the fact that the Coriolis parameter increases three times in the meridional direction; thus, there is a big difference in the basin-cross time. In fact, the basin-cross time for the first baroclinic mode of Rossby wave is about 10 months in the northern basin (approx-

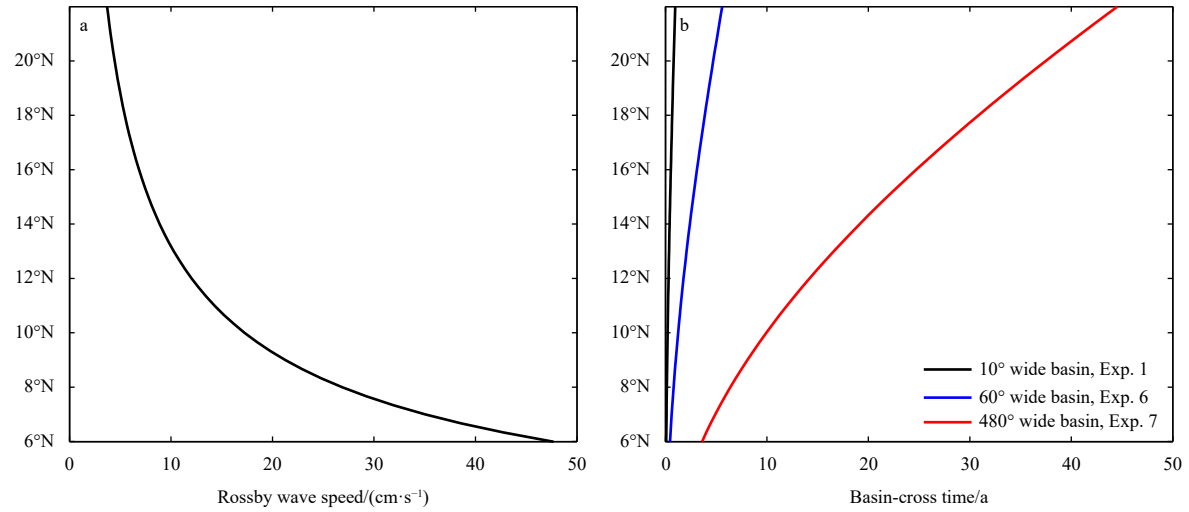

Fig. 12. Rossby wave speed (a) and the cross-basin time (b) for the models with the same meridional location, but different zonal width (Exps 1, 6, 7).

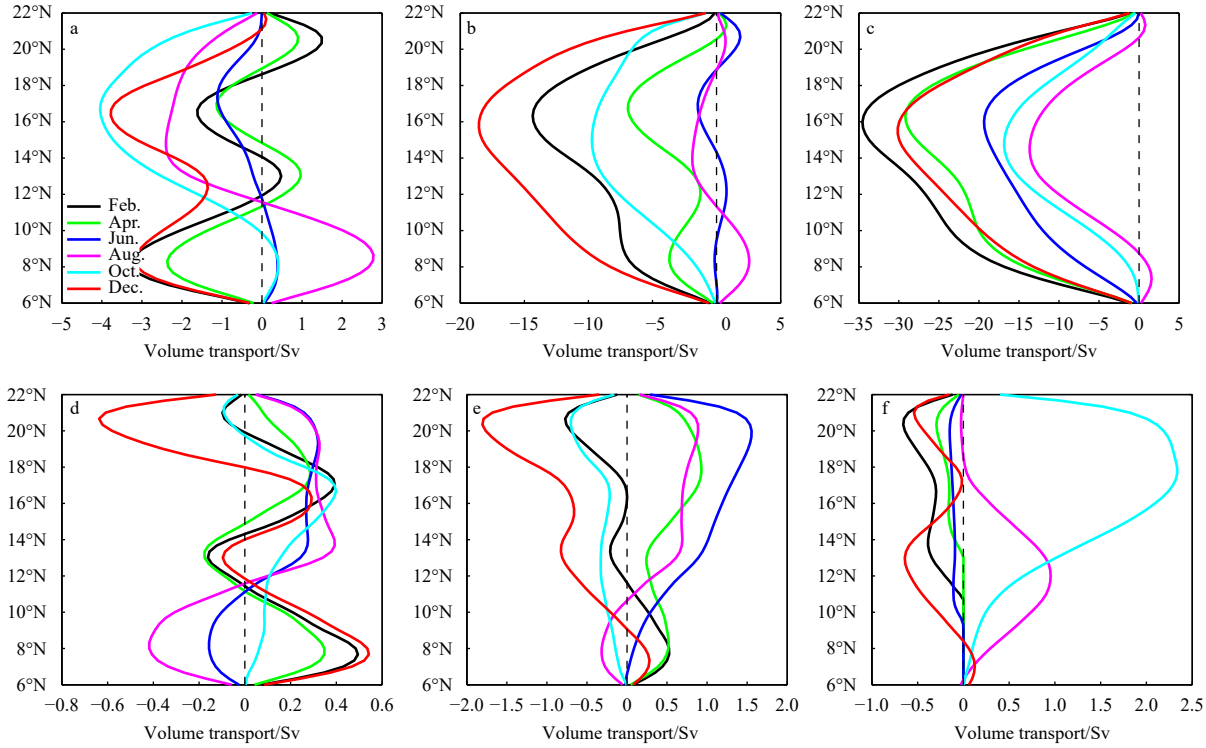

Fig. 13. Latitudinal distribution of volume transport based on models with the same meridional range of 6°–22°N, but different zonal width of 10° (Exp. 1, a, d), 60° (Exp. 6, b, e), and 480° (Exp. 7, c, f) for western boundary current (a–c) and eastern boundary current (d–f) (1 Sv=10^6 m^3/s).

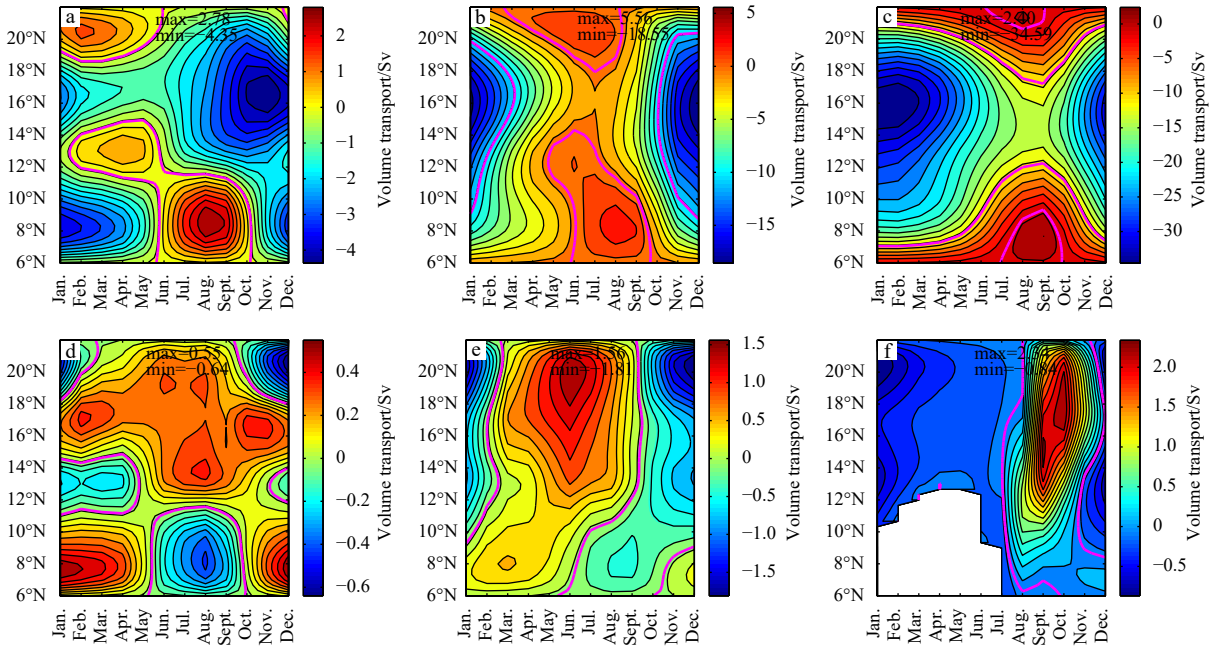

Fig. 14. Time-latitude diagram of volumetric transport of the western boundary current (a–c) and eastern boundary current (d–f) for models with the same meridional range of 6°–22°N , but different zonal width of 10° (Exp. 1, a, d), 60° (Exp. 6, b, e), and 480° (Exp. 7, c, f). The magenta curves indicate the zero contours (1 Sv=10^6 m^3/s).

imately around 22°N); in comparison, it is as short as 1–2 months in the southern basin (approximately around 6°N). The combination of these two leads to a strong seasonal cycle of the circulation in the SCS. Therefore, circulation properties for a station in the model ocean are not solely determined by the forcing at that time instance only; instead, they depend on the information over the past months, as demonstrated by Eq. (13). Both the corresponding eastern boundary layer thickness at the previous time and the delayed Sverdrup term integrated over the past months contribute to the regulation of circulation properties in the basin interior. As a result, the circulation in the SCS is in a state of forced oscillation.

In departure of the steady wind-driven circulation discussed in many existing textbooks, the circulation in the SCS is characterized by the imbalance of mechanical energy and vorticity for the whole basin at any part of the seasonal cycle. In particular, the western boundary current in the SCS cannot balance the mass, mechanical energy and vorticity in the seasonal cycle of the basin. Consequently, the circulation near the western boundary cannot be interpreted in terms of the wind stress and thermohaline forcing at the same time. Instead, circulation properties near the western boundary should be interpreted in terms of the contributions due to the delayed wind stress and the eastern boundary layer thickness.

What we learn from this simple model ocean for SCS with closed lateral boundary may also have important implication for the circulation in the Indian Ocean, where the wind stress forcing has very strong annual cycle dominated by the Indian monsoon.

Acknowledgements

We thank Xueqi Liu for helping the data processing. We appreciate three anonymous reviewers for their valuable comments.

References

Cai Shuqun, Long Xiaomin, Wu Renhao, et al. 2008. Geographical and monthly variability of the first baroclinic Rossby radius of deformation in the South China Sea. Journal of Marine Systems, 74(1–2): 711–720, doi: 10.1016/j.jmarsys.2007.12.008

Chu P C, Edmons N L, Fan Chenwu. 1999. Dynamical mechanisms for the South China Sea seasonal circulation and thermohaline variabilities. Journal of Physical Oceanography, 29(11): 2971–2989, doi: 10.1175/1520-0485(1999)029<2971:DMFTSC>2.0.CO;2

Fang Wendong, Fang Guohong, Shi Ping, et al. 2002. Seasonal structures of upper layer circulation in the southern South China Sea from *in situ* observations. Journal of Geophysical Research: Oceans, 107(C11): 3202, doi: 10.1029/2002JC001343

Gan Jianping, Li H, Curchitser E N, et al. 2006. Modeling South China Sea circulation: Response to seasonal forcing regimes. Journal of Geophysical Research: Oceans, 111(C6): C06034

He Zhigang, Lyu Kewei, Quan Qi. 2020. The South China Sea western boundary current. In: Hu J, Ho C R, Xie L, et al., eds. Regional Oceanography of the South China Sea. Singapore: World Scientific, 77–99

Huang Rui xin. 1986. Numerical simulation of wind-driven circulation in a subtropical/subpolar basin. Journal of Physical Oceanography, 16(10): 1636–1650, doi: 10.1175/1520-0485(1986)016<1636:NSOWDC>2.0.CO;2

Huang Rui xin. 2010. Ocean Circulation: Wind-Driven and Thermohaline Processes. Cambridge: Cambridge University Press

Liang Xiangshan. 2017. The seasonally varying monsoon wind may suppress the western boundary current in the South China Sea. Oceanography & Fisheries Open Access Journal, 3(1): 555601

Pedlosky J. 1965. A study of the time dependent ocean circulation. Journal of the Atmospheric Sciences, 22(3): 267–272, doi: 10.1175/1520-0469(1965)022<0267:ASOTTD>2.0.CO;2

Qu Tangdong. 2000. Upper-layer circulation in the South China Sea. Journal of Physical Oceanography, 30(6): 1450–1460, doi: 10.1175/1520-0485(2000)030<1450:ULCITS>2.0.CO;2

Shaw P T, Chao S Y, Fu L L. 1999. Sea surface height variations in the South China Sea from satellite altimetry. Oceanologica Acta, 22(1): 1–17, doi: 10.1016/S0399-1784(99)80028-0

Stommel H. 1948. The westward intensification of wind-driven ocean

currents. Eos, Transactions American Geophysical Union, 29(2): 202–206

Wang Guihua, Chen Dake, Su Jilan. 2006. Generation and life cycle of the dipole in the South China Sea summer circulation. Journal of Geophysical Research: Oceans, 111: C06002

Wyrtki K. 1961. Physical oceanography of the Southeast Asian waters. La Jolla: The University of California

Yang Haijun, Liu Qinyu. 2003. Forced Rossby wave in the northern South China Sea. Deep-Sea Research Part I: Oceanographic Research Papers, 50(7): 917–926, doi: 10.1016/S0967-0637(03)00074-8

Yang Haijun, Liu Qinyu, Liu Zhengyu, et al. 2002. A general circulation model study of the dynamics of the upper ocean circulation of the South China Sea. Journal of Geophysical Research: Oceans, 107(C7): 22-1–22-14

Yang Jiayan, Price James F. 2000. Water-mass formation and potential vorticity balance in an abyssal ocean circulation. Journal of Marine Research, 58: 789–808.

Appendix: The delayed Sverdrup relation

For the wind-driven circulation, the long Rossby waves forced by wind stress imposed on the surface are the key player in regulating the circulation. To derive the suitable relations, we start from the linearized equations of a reduced gravity model, dropping the time-dependent terms in the momentum equation and the friction terms; thus, we have

$$-fv = -g'\frac{\partial h}{\partial x} + \tau^x/\rho_0 H, \tag{A1}$$

$$fu = -g'\frac{\partial h}{\partial y} + \tau^y/\rho_0 H. \tag{A2}$$

Cross-differentiating Eqs (A1) and (A2), then subtracting and substituting into Eq. (A3) leads to a simple relation for the layer thickness propagation.

$$\frac{\partial h}{\partial t} + H\left(\frac{\partial u}{\partial x} + \frac{\partial v}{\partial y}\right) = 0, \tag{A3}$$

$$\frac{\partial h}{\partial t} - C(y)\frac{\partial h}{\partial x} = -w_e, \tag{A4}$$

where

$$C(y) = \frac{\beta g' H}{f^2},\ w_e = \frac{1}{f\rho_0}\left(\frac{\partial \tau^y}{\partial x} - \frac{\partial \tau^x}{\partial y} + \frac{\beta \tau^x}{f}\right) \tag{A5}$$

are the speed of long baroclinic Rossby waves and the corresponding Ekman pumping rate induced by wind stress. Introducing the following coordinate transform

$$t = (\xi + \eta)/2,\ x = C(y)(\xi - \eta)/2, \tag{A6}$$

$$\xi = t + x/C(y),\ \eta = t - x/C(y), \tag{A7}$$

Eq. (A4) is reduced to

$$\frac{\partial h}{\partial \eta} = -\frac{1}{2}w_e\left(C(y)\frac{\xi - \eta}{2}, y, \frac{\xi + \eta}{2}\right), \tag{A8}$$

this leads to

$$h = h(\xi, y, \eta_e) - \frac{1}{2}\int_{\eta_e}^{\eta} w_e(\xi, y, \eta)\,\mathrm{d}\eta, \tag{A9}$$

or the final form

$$h = h\left(x_e, y, t + \frac{x - x_e}{C(y)}\right) - \frac{f^2}{\beta g' H}\int_x^{x_e} w_e\left(x', y, t + \frac{x - x'}{C(y)}\right)\mathrm{d}x'. \tag{A10}$$